Mon. Not. R. Astron. Soc. **338,** 880–890 (2003)

# The effects of mergers on the formation of disc–bulge systems in hierarchical clustering scenarios

C. Scannapieco[1⋆] and P. B. Tissera[1,2]

[1]*Instituto de Astronomía y Física del Espacio, IAFE, Casilla de Correos 67, Suc. 28, Buenos Aires 1428, Argentina*
[2]*Consejo Nacional de Investigaciones Científicas y Técnicas, CONICET, Argentina*

Accepted 2002 September 30. Received 2002 September 27; in original form 2002 July 4

**ABSTRACT**

We study the effects of mergers on the structural properties of disc-like systems by using smooth particle hydrodynamical (SPH) numerical simulations in hierarchical clustering scenarios. In order to assess the effects of mergers on the mass distributions we performed a bulge–disc decomposition of the projected surface density of the systems at different stages of the merger process. We assumed an exponential law for the disc component and the Sérsic law for the bulges. We found that simulated objects at $z = 0$ have bulge profiles with shape parameters $n \approx 1$, consistent with observational results of spiral galaxies. The complete sample of simulated objects at $z = 0$ and $z > 0$ shows that $n$ takes values in the range $n \approx 0.4$–4. We found that secular evolution tends to produce exponential bulge profiles, while the fusion of baryonic cores tends to increase the $n$ value and helps to generate the correlation between $B/D$ and $n$. We found no dependence on the relative mass of the colliding objects. Our results suggest that mergers, through secular evolution and fusions, could produce the transformation of galactic objects along the Hubble sequence by driving a morphological loop that might also depend on the properties of the central galactic potential wells, which are also affected by mergers.

**Key words:** methods: numerical – galaxies: evolution – galaxies: fundamental parameters – galaxies: interactions.

## 1 INTRODUCTION

The origin of the Hubble sequence is still a controversial issue. In particular, spiral galaxies seem to evolve along this phenomenological classification although the physical mechanisms behind these morphological changes are not fully understood. The structural parameters, the gas abundances and the star formation activity vary along galaxies in the Hubble sequence in the sense that disc-dominated systems are also the more gaseous ones, experiencing on-going star formation. The large data base of galaxies gathered in recent years have allowed us to obtain more detailed information on the properties of galaxies of different morphological types in the local Universe.

Observational results show that when a double exponential decomposition is applied to the surface luminosity density of late-type spirals, the scalelengths of the bulge and disc components seem to be restricted to a certain value $\langle r_b/r_d \rangle \approx 0.10$ (Courteau, de Jong & Broeils 1996, hereafter CdJB96). This restriction in the range of possible scalelengths for spirals has been interpreted as proof of secular evolution being the mechanism responsible for bulge formation from an already in place disc structure. Recently, MacArthur, Courteau & Holtzman (2002, hereafter MCH02) studied a larger sample of late-type spirals and carried out a bulge–disc decomposition assuming a Sérsic law for the bulge surface luminosity density. These authors found a continuous distribution of the shape parameter of the bulge ($n \approx 0.2$–2) with a maximum at $n \approx 0.90$. They also found a restricted range of values for the scalelengths of the bulge and disc when the shape parameter is $n \approx 1$, $\langle r_b/r_d \rangle = 0.13 \pm 0.06$ in the $R$ band. Previous works have also found that bulges of spirals can be fitted by a Sérsic law with different shape parameters (e.g. Andredakis, Peletier & Balcells 1995, hereafter APB95; Khosroshahi, Wadadekar & Kembhavi 2000, hereafter KWK00; Graham & de Blok 2001, hereafter GdB01). APB95 and GdB01 also found a correlation between the luminosity bulge-to-disc ratio $B/D$ and the shape parameter of the bulge, which also correlates with morphological type. These observational results suggest a possible connection between the formation of the bulge and disc components. They also support the idea that $n$ could be used as a good indicator of position in the Hubble sequence.

Several theories have been developed to explain the formation of the disc and bulge components. In the case of the disc systems, the standard model is based on three hypotheses: the angular momentum is acquired through cosmological torques (Peebles 1969), baryons and dark matter have the same specific angular momentum content ($J$), and this specific angular momentum is conserved during the collapse and cooling of baryons (Fall & Efstathiou 1980,

⋆E-mail: cecilia@iafe.uba.ar

hereafter FE80). This model has been successful in reproducing several observational results in analytical and semi-analytical models (e.g. Dalcanton, Spergel & Summers 1997; Mo, Mao & White 1998). However, serious problems arose in numerical simulations where an important angular momentum transfer from baryons to the dark matter haloes during mergers was detected, breaking the condition of $J$ conservation. Domínguez-Tenreiro, Tissera & Sáiz (1998, hereafter DT98) showed that a disc-like structure with observational counterpart (Sáiz, Domínguez-Tenreiro & Tissera 2001, hereafter S01) can be built up if a compact stellar bulge is allowed to form without depleting the gas reservoir of the system. These stellar bulges provide stability to the gaseous disc systems, which are capable of conserving a non-negligible fraction of its angular momentum during violent events. Supernova energy feedback could also contribute to the formation of the disc component, regulating the star formation rate and preventing early catastrophic depletion of the gas into stars. Probably both mechanisms, the formation of a compact stellar bulge that ensures the axisymmetrical character of the potential well and energy feedback, work together in nature to allow the formation of spiral galaxies (e.g. Weil, Eke & Efstathiou 1998).

The formation of bulges is a more complex task since several mechanisms could be acting together such as monolithic collapse (Gilmore & Wyse 1998), mergers (Kauffmann, Guiderdoni & White 1994) and secular evolution (Pfenniger & Norman 1990). In general, analytical models and pre-prepared simulations have focused in one or two of them at the time (e.g. van den Bosch 1999; Aguerri, Balcells & Peletier 2001, hereafter A01). These models have been successful in explaining some properties of spiral galaxies, despite their approximations.

The current paradigm for the formation of the structure favours a hierarchical clustering scenario where the structure forms by aggregation of substructure. Hence, a galactic object experiences the effects of collapse, merger, interaction and probably secular evolution in a non-simple fashion, which can also depend strongly on redshift. In particular, violent events (i.e. mergers, interactions) can have important effects on the internal properties of the objects, such as their mass distribution (Mihos & Hernquist 1996) and star formation activity (Tissera et al. 2002, hereafter T02).

Minor and major mergers of disc systems with satellites have been studied extensively. However, most of these works do not consider the presence of the stellar bulges. The relevance of this component in the overall evolution of a disc system during a merger has been first pointed out by Mihos & Hernquist (1994) in a study of pre-prepared mergers. Recently, A01 studied the effects of mergers on the structural parameters of bulges of disc-like systems by assuming that initially bulges form with an exponential profile. These authors found that collisionless mergers produce a migration to higher $n$ and that this effect is proportional to the relative mass of the colliding systems. The simulations used in this analysis were non-cosmological pre-prepared ones where ongoing star formation and gas dynamics were not included. Recently, T02 show for the first time in cosmological smooth particle hydrodynamical (SPH) simulations how the central mass concentration in disc-like systems can grow by collapse, merger and secular evolution.

These numerical results suggest that a key point in the formation of both bulges and discs in hierarchical clustering scenarios seems to be mergers. Mergers have been traditionally suggested as a possible mechanism to drive the Hubble sequence since they can modify the dynamical and astrophysical properties of galactic objects. Hence, the question would be how, in hierarchical scenarios, do mergers work to shape disc-like objects and whether the properties of these objects resemble those of current spirals. In this paper we will focus on the analysis of the mass distributions of disc-like systems and how they are modified during mergers, paying special attention to the comparative study of the effects of secular evolution triggered by tidal fields and of the actual collision of the baryonic clumps. In order to assess the effects of mergers on the mass distributions we perform a bulge–disc decomposition of the projected surface density of the systems at different stages of the merger process. We then study how such different structural parameters, including the shape parameter defined by Sérsic (1968), evolve during the orbital decay phase and fusion of the satellite.

Our simulations include the effects of gravitation, hydrodynamics, cooling and star formation within a cosmological framework. Hence, the set of mergers that we analyse are given by the particular evolutionary history of each galactic object. This is a crucial point since the merger parameters and physical characteristics of the colliding objects are not ad hoc choices but result from the consistent formation of the structure in a hierarchical scenario. The drawback of our approach is a lower numerical resolution compared with those used in studies of pre-prepared mergers. An assessment of possible numerical problems is discussed throughout the paper.

In Section 2 we present the analysis of the simulations. In Section 3 we discuss the results. Section 4 summarizes the conclusions.

## 2 MODELS AND ANALYSIS

We run cosmological SPH simulations that include hydrodynamics and star formation (Tissera, Lambas & Abadi 1997). The simulated boxes represent typical regions of a standard cold dark matter (CDM) universe of side $5\ h^{-1}$ Mpc and $64^3$ particles ($\Omega = 1$, $\Lambda = 0$, $h = 0.5$). We assume a baryonic density parameter of $\Omega_b = 0.10$. All baryonic and dark matter particles have the same mass, $M_p = 2.6 \times 10^8\ M_\odot$. We have used a gravitational softening of 3.0 kpc and a minimum hydrodynamical smoothing length of 1.5 kpc. We performed three simulations with different realizations of the power spectrum (cluster normalized) and the same cosmological and star formation parameters. The simulated volume is the result of a compromise between the need to have a well-represented galaxy sample and enough numerical resolution to study the astrophysical properties of the simulated galaxies. We are confident that since we focus our analysis on small-scale processes such as mergers and interactions, scale fluctuations of the order of the box size will have no significant effect on such local processes. Also note that we are interested in the effects that mergers have on the mass distributions of the galactic objects analysing them as individual events and not in connection with their evolution or environment.

The star formation algorithm used in these models is based on the Schmidt law (see Tissera et al. 1997 for details). Cold gas particles are eligible to form stars if they are denser than a certain critical value and satisfy the Jeans instability criterion (Navarro & White 1994). Gas particles are checked to make sure they satisfy these conditions at all integration time-steps. Hence, as the gas cools down and is gathered at the centre of dark matter haloes, it is gradually transformed into stars according to the particular history of evolution of each galactic object. Only one free parameter has to be fixed: the star formation efficiency, which links the dynamical time of the gas cloud represented by a particle with its star formation time-scale. We have used the value adopted by S01 since it is adequate to reproduce disc-like structures with observational counterparts at $z = 0$. These authors used a low star formation efficiency that allows the formation of a stellar bulge that ensures the axisymmetrical character of the potential well but without exhausting the gas reservoir (see also

DT98). Consequently, disc-like structures can be formed, although they remain mainly gaseous. Conversely, observed discs are mostly stellar, but they inherit the structural and dynamical properties of the gaseous discs out of which disc stars are formed. Hence, for the sake of comparison, the values of the parameters describing these properties can be reliably estimated from the simulated gaseous discs. In this paper, we will determine and use these parameters to study the effects of mergers on the mass distribution of the simulated galactic objects.

At $z = 0$, we identify galactic objects at their virial radius, analysing only those with more than 4000 dark matter particles within their virial radius in order to diminish numerical resolution problems. Within each galactic object, a main baryonic clump is individualized which, hereafter, will be called the galaxy-like object (GLO).

The selected GLOs have very well-resolved dark matter haloes that provide adequate potential wells for baryons to collapse in. This fact ensures a reliable description of the gas density profiles (see Steinmetz & White 1997), which allows us to follow the star formation history of the GLOs (see Tissera 2000). With this strong restriction on the minimum number of particles, the final GLO sample at $z = 0$ is made up of 12 GLOs with virial velocities in the range 140–180 km s$^{-1}$.

We follow the evolution of the selected GLOs with look-back time [$\tau(z) = 1 - (1 + z)^{-3/2}$] identifying mergers and starbursts (SBs). We then construct their mergers trees and star formation rate (SFR) histories (because of the restrictive SF efficiency used, these SFR histories are mainly those of the bulge components). During a merger event, the progenitor object is chosen as the more massive baryonic clump within this merger tree, while the minor colliding baryonic clump is referred to as the satellite. Following T02 we study only those mergers that are directly linked to starbursts in the SF history of each GLO. These authors found that during the orbital decay phase of some merger events, early gas inflows that trigger star formation can develop. In this case, if the gas reservoir of the GLOs is not exhausted during these starbursts, second bursts are induced at the actual physical contact of the baryonic clumps. The induction of early gas inflows could be directly linked to the properties of the total potential wells of the systems in agreement with previous results reported by Barnes & Hernquist (1996) and Mihos & Hernquist (1996) in pre-prepared simulations. When no gas inflows are triggered during the orbital decay phase (ODP), only one SB is detected when the two baryonic clumps collide. These events will be called single SBs (SSBs), while those where two SBs are detected will be called double SBs (DSBs). We studied a total of 18 merger events with merger parameters settled by the cosmological model. Among them, 11 are classified as DSBs and seven as SSBs. Fig. 1 shows an example of both types of SBs. We have also plotted the distance between the centres of mass of the progenitor and the satellite since the redshift they share the same dark matter halo. The merger event will be determined by four redshifts of reference, $z_A$: the beginning of the first bursts in DSBs and the ODP in SSBs, $z_B$: the end of both the first bursts in DSBs and the ODP in SSBs, $z_C$: the beginning of the second SBs in DSBs and the only bursts in SSBs (in this case $z_B = z_C$), and $z_D$: the end of the second bursts in DSBs and of the only one in SSBs. These redshifts have been depicted in Fig. 1. Note that the ODP, defined as the time since two objects share the same dark matter halo to the fusion of their main baryonic cores, is determined by $z_A$ and $z_C$. The $z_B$ redshift is used in the case of DSBs since it establishes the end of the first SBs.

In order to quantify the changes in the baryonic mass distributions, we carried out a bulge–disc decomposition of the projected mass

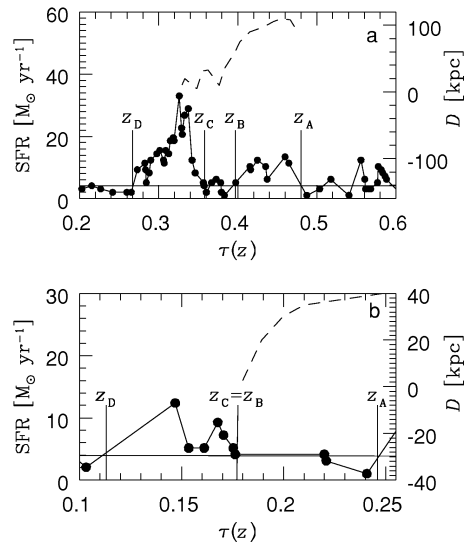


**Figure 1.** Star formation rate for typical galaxy-like objects during a double starburst (a) and a single one (b) as a function of look-back time [$\tau(z)$]. The solid lines represent the ambient star formation components and the dashed lines depict the distance between the mass centres of the progenitors and satellites ($D$). The four redshifts of interest during a merger event have also been plotted.

surface density of the GLOs at $z = 0$ and of the progenitors at each of the redshifts that define a merger event. We assumed an exponential profile for the disc component and the Sérsic law for the bulge central mass concentration:

$$\Sigma_d = \Sigma_d^o \exp[-(r/r_d)] \quad (1)$$

$$\Sigma_b = \Sigma_b^o \exp\left[-(r/r_b)^{1/n}\right], \quad (2)$$

where $r_d$ and $r_b$ are the disc and bulge scalelengths, $\Sigma_d^o$ and $\Sigma_b^o$ are the corresponding central mass surface densities and $n$ is the bulge shape parameter.

For each GLO at $z = 0$ and its progenitor objects, we estimated the total angular momentum ($j$) and projected the mass distribution on to the perpendicular plane defined by $j$. We then integrated the projected baryonic mass in concentric cylinders of radius $r$ since, as has been proved by S01, it is numerically more convenient to fit the integrated mass than the surface density. In order to diminish the effects of numerical resolution, the fits were made from $r = 1.5$ kpc to $r \approx 30$ kpc, except in those cases where the mass distributions of the progenitors were strongly perturbed by the entrance of the satellites.

The total integrated baryonic mass of the GLOs ($M_{GLO}$) is estimated, on one hand, as the baryonic mass within $r = 30$ kpc, and will be associated with the luminous galaxy. On the other hand, $M_{GLO}$ is the result of the disc ($M_d$) and bulge ($M_b$) mass contributions:

$$M_{GLO} = M_d + M_b \quad (3)$$

$$M_d = 2\pi\Sigma_d^o r_d^2 \quad (4)$$

$$M_b = 2\pi\Sigma_b^o r_b^2 n\Gamma(2n), \quad (5)$$

where $\Gamma$ is the complete gamma function. Since $M_{GLO}$ is known, there are four free parameters to be fitted: $r_d$, $r_b$, $\Sigma_b^o$ (or $\Sigma_d^o$) and $n$. From these fitted parameters we analyse possible correlations with the dynamical and astrophysical properties of the GLOs and their

dark matter haloes. In particular, we will study how the structural parameters change during merger events.

Note that we work with masses instead of luminosities, and hence the mass-to-light ratios for the bulge and disc components will have to be adopted in order to be able to compare our results with observations. To this end we use different observational results from APB95 (30 S0–Sbc galaxies in the *K* band), CdJB96 (173 spiral Sb–Sc galaxies in the deep *R* band), Moriondo, Giovanelli & Haynes (1999, hereafter MGH99, 25 Sa–Scd spiral galaxies in the *K* band), KWK00 (27 early-type disc galaxies in the *K* band) and MCH02 (47 late-type spiral galaxies in the *R* band). APB95, KWK00 and MCH02 used bulge–disc decompositions of the luminosity surface density profiles, allowing the bulge shape parameter to vary. CdJB96 used double-exponential fittings ($n = 1$). Finally, MGH99 made fittings with different $n$ values, finding that most of their bulges were better described by $n = 1$ (except for two with $n = 2$). Note that all of these observations correspond to galaxies at $z \approx 0$.

## 3 RESULTS

### 3.1 GLOs at $z = 0$

As we mentioned before, S01 showed that disc-like objects formed in numerical simulations where stellar bulges were allowed to form have structural parameters and specific angular momentum content similar to those of observed spiral galaxies. For the sake of completeness and to show that these findings are valid for our GLOs, we will first discuss their properties at $z = 0$. The structural parameters and the circular velocity [$V^2 = GM(r)/r$] at $r = 2.2r_{\rm d}$ allow the classification of our objects as intermediate spirals ($100 \leqslant V_{2.2} \leqslant 180$ km s$^{-1}$; four GLOs), bright spirals ($V_{2.2} > 180$ km s$^{-1}$ and $r_{\rm d} > 5.25$ kpc; two GLOs) and compact bright spirals ($V_{2.2} > 180$ km s$^{-1}$ and $r_{\rm d} < 5.25$ kpc; six GLOs). This is the result of our strong condition on the mass of GLOs in order to work with those that are better resolved.

In Fig. 2 we show the relation between the disc and bulge scalelengths. Each GLO has a label that specifies its $n$ shape parameter. We include the observational data from CdJB96, MGH99, KWK00 and MCH02. Note that for increasing $n$ parameters, the scalelengths tend to move to the upper envelope of the distribution. This effect is also seen in the observed scalelength distribution. We have adopted $n = 1.5$ as a general cut-off value to segregate the samples between those with exponential and non-exponential profiles for the bulge components.

In Fig. 3 we show the normalized histogram of $n$ for GLOs at $z = 0$ (a), and the corresponding distribution for the observations of APB95, KWK00 and MCH02 (b), normalized to the total number of galaxies in each sample. The combined observational sample covers a morphological range from Sa to Sc galaxies, but this is not a consistent sample. We show it in order to broadly compare the range of $n$ values obtained from the simulations with observations. The average $n$ values over the observed subsamples are $\langle n_{\rm APB95}\rangle = 2.97 \pm 1.29$, $\langle n_{\rm KWK00}\rangle = 2.88 \pm 0.94$ and $\langle n_{\rm MCH02}\rangle = 1.02 \pm 0.43$, while the simulated sample has $\langle n_{\rm sim}\rangle = 1.23 \pm 0.40$. The simulated distribution is consistent with the observations of MCH02 at $1\sigma$ level, which suggests that our objects are more similar to late-type galaxies. However, $\langle n_{\rm sim}\rangle$ value also agrees at the $3\sigma$ level with the corresponding mean values of the early-type samples.

A key point in the formation of discs is the conservation of the specific angular momentum (FE80). Our SF algorithm has been implemented in such a way that it has allowed the formation of stellar bulges but without exhausting the gas reservoir (DT98). Hence,

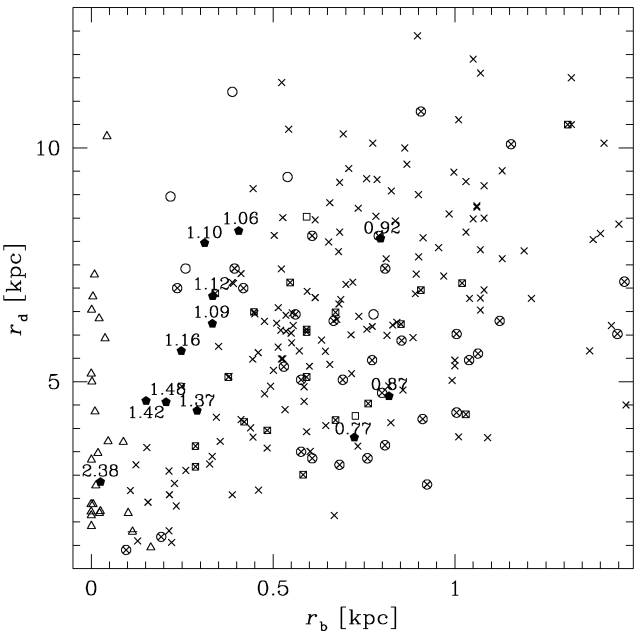


**Figure 2.** Disc scalelength ($r_{\rm d}$) as a function of bulge scalelength ($r_{\rm b}$) for simulated objects at $z = 0$ (filled pentagons). Labels with the shape parameters ($n$) of the simulated bulges are shown. Observational data from CdJB96 (crosses), MGH99 ($n = 1$ crossed squares, $n = 2$: open squares), KWK00 ($n \leqslant 1.5$: dashed triangles, $n > 1.5$: open triangles) and MCH02 ($n \leqslant 1.5$: crossed circles, $n > 1.5$: open circles) are also included.

gaseous discs have been able to regenerate after mergers. In order to compare the angular momentum ($j$) of the three mass components: bulge, disc and dark matter halo, with observations, we plot in Fig. 4 their specific angular momentum ($J = j/M$) content as a function of mass ($M$). The mass and angular momentum of bulges have been estimated with stars within $r < r_{\rm eff}$, while those of the gaseous discs have been calculated within $r < 3.2r_{\rm d}$. These criteria have been adopted following those used by observers. The mass and angular momentum of the dark matter haloes have been estimated at the virial radius. In this figure, we have also included two boxes that depict the observational region covered by spirals and ellipticals as given by Fall (1983). From this plot we can see that the disc components and the dark matter haloes have comparable specific angular momentum contents as predicted by the standard disc formation model of FE80. Conversely, stellar bulges have been formed from material that has lost most of its angular momentum.

From these results we conclude that the simulated GLOs have structural and dynamical parameters that statistically resemble those of current normal spirals at $z = 0$. In the following section we will study the role played by mergers in the determination of these properties and try to understand the origin of correlations among the structural parameters such as $B/D$ versus $n$.

### 3.2 Analysis of progenitors during merger events

We carried out the bulge–disc ($B + D$) decomposition of the progenitor objects of the GLOs analysed in the previous section during merger events at the four redshifts of interest: $z_{\rm A}$, $z_{\rm B}$, $z_{\rm C}$ and $z_{\rm D}$. In this section we will study how their structural parameters change during these processes.

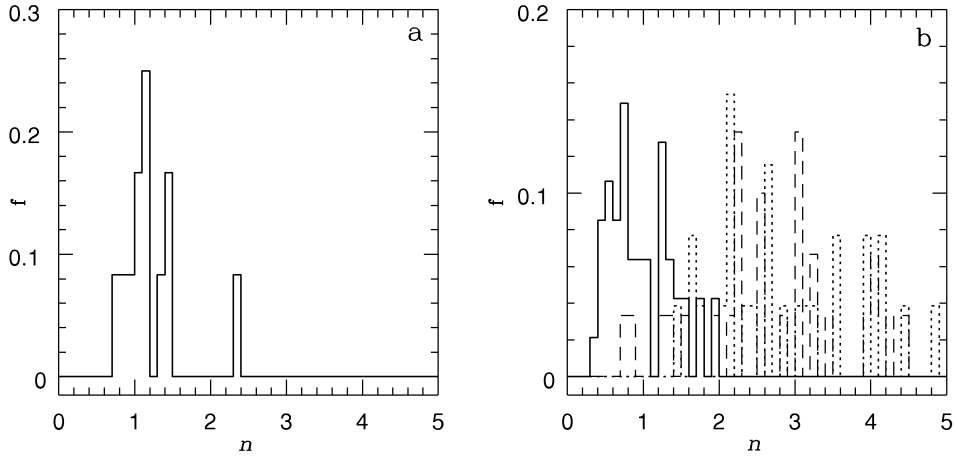


**Figure 3.** Histogram of the shape parameter of the bulges for simulated objects at $z = 0$ (a) and observations from APB95 (dashed line), KWK00 (dotted line) and MCH02 (solid line), normalized to the total number of galaxies in each sample.

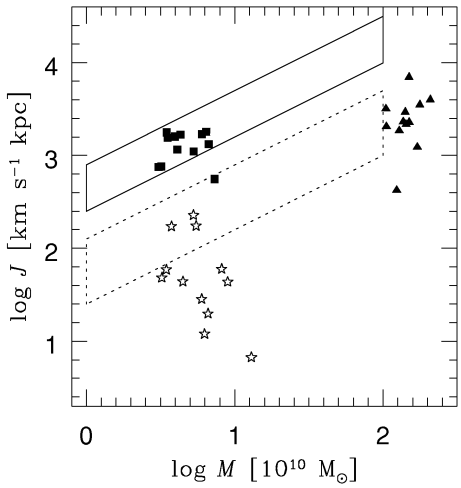


**Figure 4.** Specific angular momentum ($J$) for the gaseous discs at $3.2r_{\rm d}$ (filled squares), the stellar bulges at $r_{\rm eff}$ (open stars) and dark matter haloes at the virial radius (filled triangles), as a function of mass ($M$). The solid (dotted) box depicts the observational area for spirals (ellipticals) from Fall (1983).

### *3.2.1 The shape parameter*

In Fig. 5(a) we show the $r_{\rm d}$ versus $r_{\rm b}$ relation for all progenitors during merger events and at $z = 0$. We have also included the observational data from a B+D decomposition from MGH99, KWK00 and MCH02, and from a double-exponential decomposition by CdJB96. The combined observed sample of spirals shows a certain correlation between $r_{\rm d}$ and $r_{\rm b}$, although some of them have, for a given disc scalelength, a smaller bulge than that expected from this relation. We also note that the scalelengths of our simulated disc structures show a similar behaviour. In order to individualize which observed and simulated objects belong to each of these two distributions of scalelengths, we segregate them according to their shape parameters as shown from Figs 5(b)–(d). It is clear that as galaxies and simulated objects with large shape parameters are taken out, the relation for both, observed and simulated scalelengths, becomes better defined.

We also note that the $r_{\rm b}$ versus $r_{\rm d}$ relation for GLOs and galaxies with bulges with $n > 1.5$ shows no trend at all. It is encouraging that the observed and simulated disc structures show scalelength distributions with similar patterns, for both $n \approx 1$ or $n \neq 1$ bulge profiles. In the case of exponential bulges ($0.9 \leqslant n \leqslant 1.1$), the correlation is well defined with $\langle r_{\rm b}/r_{\rm d}\rangle = 0.14 \pm 0.05$ and $\langle r_{\rm b}/r_{\rm d}\rangle = 0.13 \pm 0.06$ for observations and simulations, respectively. Table 1 summarizes the mean values of $r_{\rm b}$, $r_{\rm d}$ and $n$ for GLOs at the four $z$ of interest.

Similarly to Fig. 3(a) we display in Fig. 6 the histogram of shape parameters for all progenitors at all studied redshifts. Hence this distribution gathers the information on the $n$ parameters of different progenitors at different stages of evolution. From the comparison with that shown in Fig. 3 corresponding to the bulges of the final structures at $z = 0$, we deduce that in the past of current GLOs, their progenitors went through stages where their bulges had $n > 1.5$ parameters (∼35 per cent of the total sample). Meanwhile, GLOs at $z = 0$ show a trend to have $n \approx 1$, with less than 10 per cent being described by $n > 1.5$.

In order to assess the effects of mergers on the shape parameters of the objects and to look for possible differences between the effects of secular evolution and fusions, we calculate the percentages corresponding to the increase and decrease of the shape parameter during the intervals $z_{\rm A}$–$z_{\rm C}$, $z_{\rm C}$–$z_{\rm D}$ and $z_{\rm A}$–$z_{\rm D}$ for SSBs and DSBs. The results are shown in Table 2. Note that we are taking the interval $z_{\rm A}$–$z_{\rm C}$ as the total period corresponding to the ODP. For both single and double SBs, we find that bulges tend to decrease their $n$ parameters during the ODP, and that this effect is more important for DSBs. In contrast, the actual fusion of the clumps ($z_{\rm C}$–$z_{\rm D}$) tends to make the $n$ value of the bulges larger.

Therefore, we find that the physical encounter of the baryonic cores tends to produce bulges with larger shape parameters (i.e. more concentrated), and $n \approx 1$ profiles tend to be formed by secular evolution. These results together with the fact that at $z = 0$ most of GLOs show $n \leqslant 1.5$, regardless of their past history, suggest that successive mergers have driven the bulges from exponential to more concentrated profiles, to come back to exponential ones, if there is available gas in the systems.

We think that the possibility of having secular evolution and core fusion associated with a merger helps to drive this cycle in the shape parameter. Note that the collisionless merger of stellar discs will not produce the same distributions. As a matter of fact, in order to detect this *morphological loop*, simulations should include gas dynamics

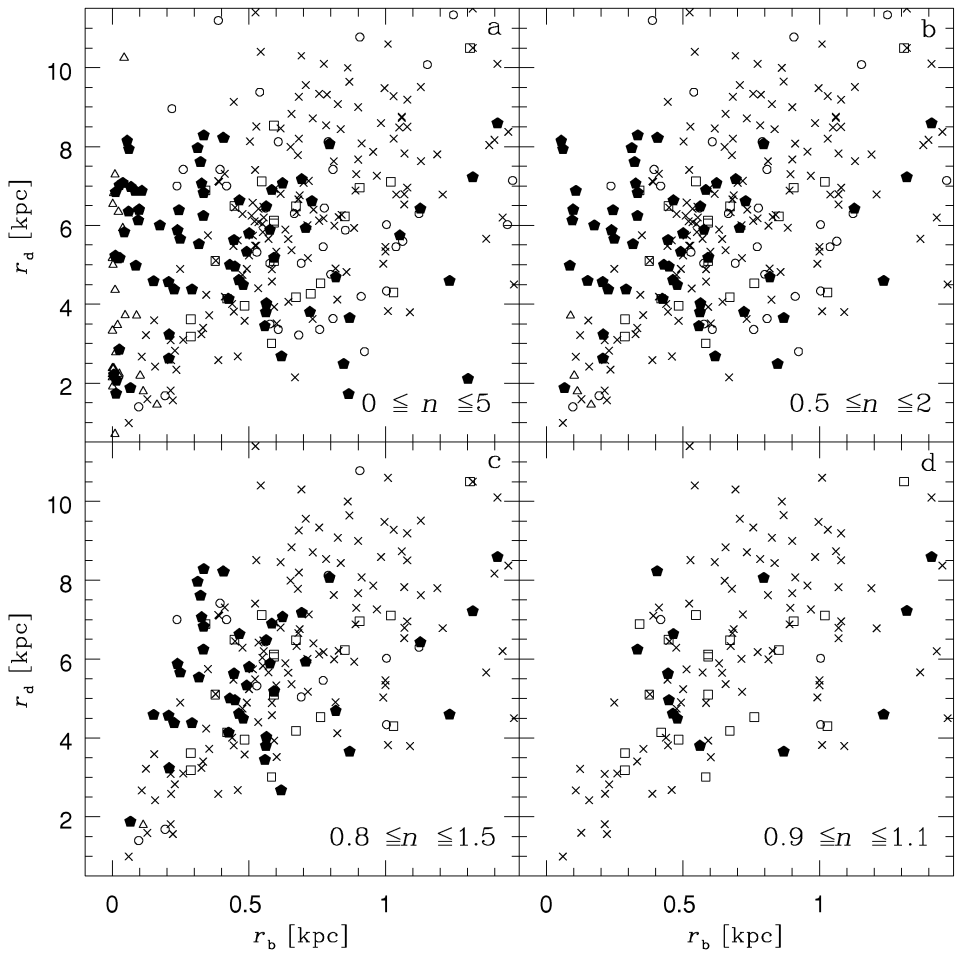


**Figure 5.** Disc scalelength ($r_d$) as a function of bulge scalelength ($r_b$) for simulated objects at $z = 0$ and progenitors (filled pentagons) for which bulges are described by $0 \leqslant n \leqslant 5$ (a), $0.5 \leqslant n \leqslant 2$ (b), $0.8 \leqslant n \leqslant 1.5$ (c) and $0.9 \leqslant n \leqslant 1.1$ (d). Observational data from CdJB96 (crosses), MGH99 (open squares), KWK00 (open triangles) and MCH02 (open circles) for the same shape parameter intervals are also shown.

**Table 1.** Mean values of bulge scalelength ($r_b$), disc scalelength ($r_d$) and bulge shape parameter $\langle n \rangle$ for single (S) and double (D) SBs for the redshifts of interest.

| $z_i$ | | $r_b$ (kpc) | $r_d$ (kpc) | $\langle n \rangle$ |
|---|---|---|---|---|
| $z_A$ | S | $0.46 \pm 0.17$ | $6.2 \pm 0.7$ | $1.5 \pm 0.2$ |
| | D | $0.31 \pm 0.11$ | $4.9 \pm 0.6$ | $1.8 \pm 0.2$ |
| $z_B$ | S | $0.57 \pm 0.16$ | $5.6 \pm 0.7$ | $1.3 \pm 0.2$ |
| | D | $0.37 \pm 0.16$ | $5.9 \pm 0.4$ | $1.6 \pm 0.2$ |
| $z_C$ | S | $0.57 \pm 0.16$ | $5.6 \pm 0.7$ | $1.3 \pm 0.2$ |
| | D | $0.53 \pm 0.12$ | $5.0 \pm 0.4$ | $1.2 \pm 0.1$ |
| $z_D$ | S | $0.52 \pm 0.12$ | $5.0 \pm 0.7$ | $1.4 \pm 0.3$ |
| | D | $0.37 \pm 0.08$ | $5.4 \pm 0.6$ | $1.4 \pm 0.2$ |

Note: The errors correspond to the bootstrap method, $\sigma_{bt}$.

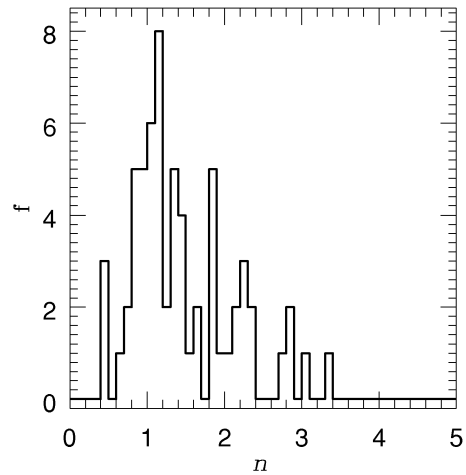


**Figure 6.** Total distribution of bulge shape parameters for the progenitors during merger events.

and star formation since, otherwise, bulges cannot be reshaped back to $n \approx 1$ (A01).

Fig. 7 shows the variations of the $n$ parameter during the ODP (a) and those produced during the fusion of the baryonic clumps (b) as a function of $M^z_{star}/M^{z=0}_{star}$, where $M^z_{star}$ is the stellar mass formed in the progenitors at $z$ and $M^{z=0}_{star}$ is the total stellar mass of the GLOs at $z = 0$. This ratio is an estimate of the presence of a stellar bulge since in these simulations the stars form preferentially in the dense regions. T02 found that the properties of the potential well can be directly linked to the stability of a system, in the sense that the shallower the potential well, the more susceptible the GLO is to experiencing early gas inflows (i.e. secular evolution). The

**Table 2.** Percentage of objects that increase ($\uparrow n$)/decrease ($\downarrow n$) their shape parameter during the ODP ($z_A$–$z_C$), the fusion of the baryonic clumps ($z_C$–$z_D$) and the whole merger process ($z_C$–$z_D$), for single (S) and double (D) starbursts.

| | | $z_A$–$z_C$ (per cent) | $z_C$–$z_D$ (per cent) | $z_A$–$z_D$ (per cent) |
|---|---|---|---|---|
| S | $\uparrow n$ | 42.9 | 57.1 | 57.1 |
| | $\downarrow n$ | 57.1 | 42.9 | 42.9 |
| D | $\uparrow n$ | 18.2 | 63.6 | 45.5 |
| | $\downarrow n$ | 81.8 | 36.4 | 54.5 |

formation of stellar bulges has been found to inhibit such early gas inflows. This picture is in agreement with our results, where the major changes in the shape parameter during a merger event correspond to the GLOs that experience DSBs ($M^z_{\rm star}/M^{z=0}_{\rm star} \leqslant 0.45$), which are less stable objects and can be strongly perturbed by the collision with a satellite. In contrast, stabler systems ($M^z_{\rm star}/M^{z=0}_{\rm star} > 0.45$) would not experience such important perturbations in its mass concentration during the ODP (Table 2).

We can also see from Fig. 7(a) that most of the changes in $n$ are negative and can be linked with smaller $M^z_{\rm star}/M^{z=0}_{\rm star}$ values ($M^z_{\rm star}/M^{z=0}_{\rm star} \leqslant 0.45$). This could be related to the fact that stellar bulges can provide stability to the systems, making them less vulnerable to the influence of a satellite, principally during the ODP. From Fig. 7(b) we see that the fusion of the baryonic cores produce more positive changes in the $n$ parameters and hence a tendency to increase it. Again, the larger variations are related to smaller bulges (i.e. smaller $M^z_{\rm star}/M^{z=0}_{\rm star}$).

We also analysed the possibility that the changes in the $n$ value during mergers are linked to the relative mass of the colliding systems, finding no correlation in contrast with the results of A01. However, these authors only considered collisionless mergers while in all our mergers dissipation plays an important role.

In Fig. 8 we have plotted the averaged $n$ parameters of the progenitors at different $z$ intervals. We can see that, although the bootstrap errors are high, there is a tendency for the averaged $n$ to decrease toward $n = 1$ for decreasing $z$. Nevertheless, at all redshifts we found the mean $n$ to be smaller than $n = 2$, indicating that, in spite of the spread of the parameters, the majority of the bulges are best fitted with $n \lesssim 1.5$.

### 3.3 The $r_b/r_d$ ratio

It has been argued by some authors (e.g. CdJB96) that there is a restricted range of $r_b/r_d$ for spiral galaxies, which has been interpreted as the result of secular evolution of the central mass concentrations. In Fig. 2 we showed the $r_d$ versus $r_b$ distribution for GLOs at $z = 0$ and for observations. We have combined the observational results from MGH99, KWK00 and MCH02, which include spiral galaxies from Sa to Sc. For these distributions we find $\langle r_b/r_d\rangle = 0.07 \pm 0.02$ (the bootstrap error is $\sigma_{bt} = 0.02$) and $\langle r_b/r_d\rangle = 0.10 \pm 0.08$ ($\sigma_{bt} = 0.01$) for the simulated and observed data, respectively, showing a good agreement.

However, we have already shown in Fig. 5 that the simulated and observed scalelength distributions show a clear trend only for those objects with bulges with $0.9 \leqslant n \leqslant 1.1$. Hence, we divided the observations and simulated data into three subsamples according to their $n$ parameters ($n < 0.9$, $0.9 \leqslant n \leqslant 1.1$ and $n > 1.1$) and estimate their mean $r_b/r_d$. Table 3 summarizes the results. First, we note that observational and simulated $\langle r_b/r_d\rangle$ in the three subsamples are in very good agreement, supporting the hypothesis that GLOs in CDM models have an observational counterpart. We also see that the larger dispersion is found for bulges with $n < 0.9$ in both the observed and simulated data, and that these subsamples show higher $\langle r_b/r_d\rangle$ than the subsamples with $n \approx 1$, suggesting that these systems systematically have larger $r_b$ (for this subsample: $\langle r_b\rangle = 0.89 \pm 0.10$ and $\langle r_d\rangle = 4.77 \pm 0.40$).

On the other hand, we find that systems with bulges better fitted by $n > 1.1$ show the smallest $\langle r_b/r_d\rangle$. Hence for a given disc scalelength, the larger the concentration of the bulges, the smaller its scalelength (for this subsample: $\langle r_b\rangle = 0.23 \pm 0.03$ and $\langle r_d\rangle = 5.52 \pm 0.30$). If we assume that the $n$ parameter correlates with morphology as is indicated by several works (e.g. de Jong 1996; Graham & Prieto 1999, hereafter GP99; GdB01), then the scalelength ratios should correlate with $n$. Fig. 9 shows the $r_b/r_d$ ratio as a function of the shape parameter for the simulated objects during mergers and for $z = 0$. We have also included observational data from KWK00 and MCH02. We find an anticorrelation between these two parameters, in agreement with observations. Assuming that the shape parameter is an indicator of Hubble type, this anticorrelation indicates that late-type spirals ($n \leqslant 1.5$) have larger $r_b/r_d$ ratios than early-type spirals ($n > 1.5$). We also note that the relation for the observed and

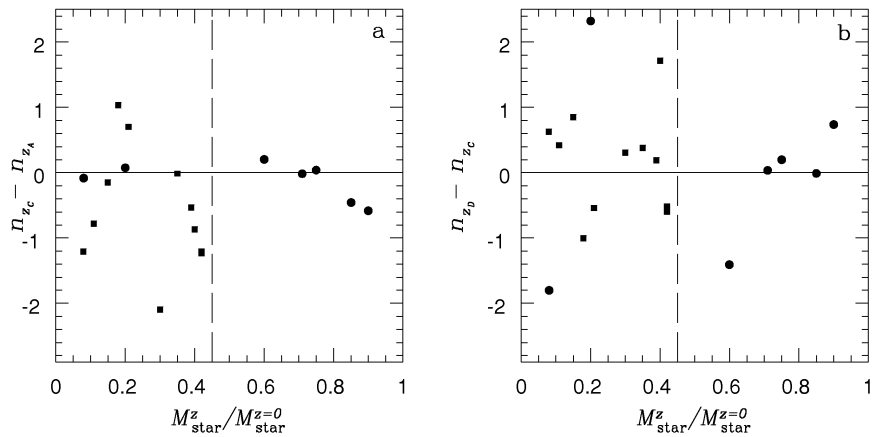


**Figure 7.** Variations in the shape parameter of the progenitors during the orbital decay phase (a) and during the fusion of the baryonic clumps (b) in single (filled circles) and double (filled squares) SBs, as a function of the fraction of stars already formed in the progenitors, $M^z_{\rm star}/M^{z=0}_{\rm star}$ when the mergers start. $M^z_{\rm star}/M^{z=0}_{\rm star} = 0.45$ (dashed lines) has been taken to be an indicator of the presence of a well-formed stellar bulge after T02.

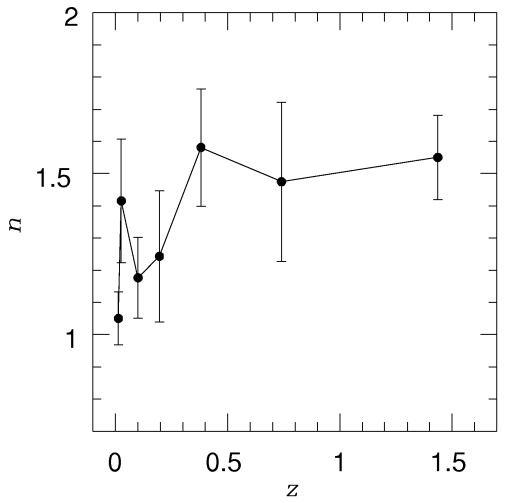


**Figure 8.** Average $n$ parameters of the progenitors at different $z$ intervals and of the GLOs at $z = 0$. The error bars correspond to the bootstrap method.

**Table 3.** Mean values of the ratio between bulge and disc scalelengths for simulations (SIM) and observations (OBS) for different cases. S and D denotes single and double SBs, respectively. The bootstrap errors are shown in brackets.

| | $\langle r_b/r_d\rangle_{SIM}$ | $\langle r_b/r_d\rangle_{OBS}$ |
|---|---|---|
| $z \neq 0$ | $0.10 \pm 0.10$ (0.01) | |
| $z = 0$ | $0.07 \pm 0.02$ (0.02) | $0.10 \pm 0.08$ (0.001) |
| $n < 0.9$ | $0.24 \pm 0.20$ (0.05) | $0.16 \pm 0.07$ (0.01) |
| $0.9 \leqslant n \leqslant 1.1$ | $0.13 \pm 0.06$ (0.02) | $0.14 \pm 0.05$ (0.02) |
| $n > 1.1$ | $0.05 \pm 0.05$ (0.01) | $0.03 \pm 0.04$ (0.01) |
| S $z_A$ | $0.07 \pm 0.05$ (0.02) | |
| S $z_D$ | $0.11 \pm 0.08$ (0.03) | |
| D $z_A$ | $0.07 \pm 0.08$ (0.02) | |
| D $z_D$ | $0.10 \pm 0.10$ (0.04) | |

simulated ratios seems to flatten for $n \ll 1$. A simple extrapolation gives a value of $r_b/r_d \approx 0.40$.

Because the shape parameter and the scalelength of the Sérsic law are coupled parameters, this trend of $r_b/r_d$ with $n$ could be the result of the fitting formula. However, Trujillo, Graham & Caon (2001, hereafter TGC01) argued that there is a physical trend stronger than that resulting from the fitting formula. Because we use the same expression for all fittings, the fact that there is a segregation in the scalelength distribution according to the value of $n$ suggests that this trend could have a physical basis and could be related to a difference in the evolution of the GLOs or in the efficiency of some physical process. This is confirmed when $r_{eff}$ is used instead of $r_b$ for which we find $\langle r_{eff}/r_d\rangle = 0.29$ ($\sigma_{bt} = 0.04$) for $n < 0.9$, $\langle r_{eff}/r_d\rangle = 0.26$ ($\sigma_{bt} = 0.03$) for $0.9 \leqslant n \leqslant 1.1$ and $\langle r_{eff}/r_d\rangle = 0.30$ ($\sigma_{bt} = 0.05$) for $n > 1.1$ [the combined observational sample of KWK00 and MCH02 shows $\langle r_{eff}/r_d\rangle = 0.23$ ($\sigma_{bt} = 0.02$) for $n < 0.9$, $\langle r_{eff}/r_d\rangle = 0.28$ ($\sigma_{bt} = 0.04$) for $0.9 \leqslant n \leqslant 1.1$, and $\langle r_{eff}/r_d\rangle = 0.35$ ($\sigma_{bt} = 0.03$) for $n > 1.1$]. We have used the approximation of Ciotti & Bertin (1999) to transform simulated $r_b$ into $r_{eff}$.

Let us now look at the mean $\langle r_b/r_d\rangle$ during mergers. In Table 3 we show the mean $r_b/r_d$ at $z_A$ and $z_D$ for SSBs and DSBs. We find no differences between the mean $r_b/r_d$ but both samples agree in increasing the mean ratios and the dispersions at $z_D$. Fig. 10 shows the distributions of scalelength during mergers. Note that, independently of the stage of evolution of the mergers, the distributions

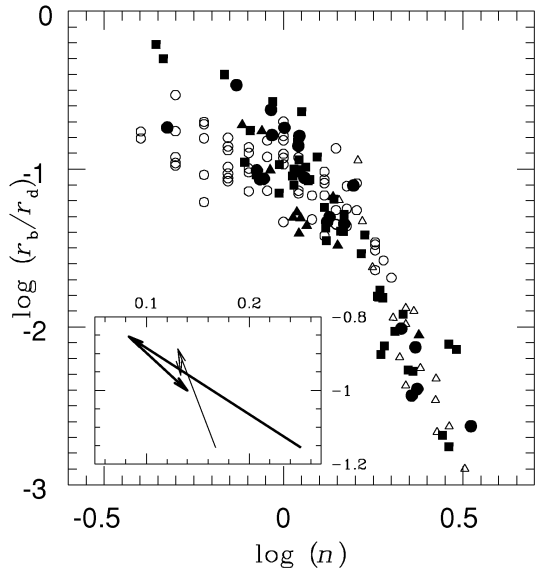


**Figure 9.** Ratio between the bulge and the disc scalelengths as a function of the bulge shape parameter for simulated objects at $z = 0$ (filled triangles), single SBs (filled circles) and double ones (filled squares). Observational data from KWK00 (open triangles) and MCH02 (open circles) are also shown. The minor box shows the changes of the plotted parameters for single (thin line) and double (thick line) SBs during the orbital decay phase (first arrow) and the fusion of the baryonic clumps (second arrow).

have similar characteristics and are within the observed range at $z = 0$. Finally, in Fig. 9, in the small box, we show how the averaged $r_b/r_d$ moves throughout mergers associated with single (thin line) and double (thick line) starbursts. It is clear that early gas inflows during the ODP tend to decrease $n$ in both cases but for DSBs the changes are more important, as expected from their stability properties (see Fig. 7 and T02). Conversely, the fusion of the cores moves the distribution toward higher $\langle n\rangle$.

### 3.4 The $B/D$ ratio

The luminosity $B/D$ ratio has been traditionally used as an indicator of morphology (e.g. Andredakis & Sanders 1994). The correlation between $B/D$ and $n$ has been shown by APB95 and recently confirmed by TGC01. Linear regression through observations show $\partial(B/D)/\partial n = 1.0 \pm 0.3$ ($\sigma_{bt} = 0.3$) for APB95, $0.8 \pm 0.5$ ($\sigma_{bt} = 0.5$) for KWK00 and $1.7 \pm 0.3$ ($\sigma_{bt} = 0.3$) for MCH02. The combined sample has $\partial(B/D)/\partial n = 1.2 \pm 0.1$ ($\sigma_{bt} = 0.1$).

Note that in the models we have masses instead of luminosities and that the mass-to-light ratios of the discs ($\gamma_d$) and bulges ($\gamma_b$) could be different because of their different stellar populations. However, their correct values and/or possible dependence on radius and redshift are still unclear. In order to match the luminosity $B/D$ we have to rescale the mass $B/D$ ratio by a constant factor of 20. We address that we are using the same mass-to-light ratios for all GLOs regardless of the redshift,[1] disc scalelength or observational band.

[1] Nevertheless, we found that very similar $\gamma_b/\gamma_d$ ratios are needed to match the observed luminosity $B/D$ for progenitors at different $z$, although our dispersion is quite high. Note that we have used the total baryonic masses to estimate luminosities. In a more realistic model including energy feedback, some fraction of the cold gas would be reheated. Hence, the values required for our models to match the observed luminosities could be taken as upper limits to the mass-to-light ratios.

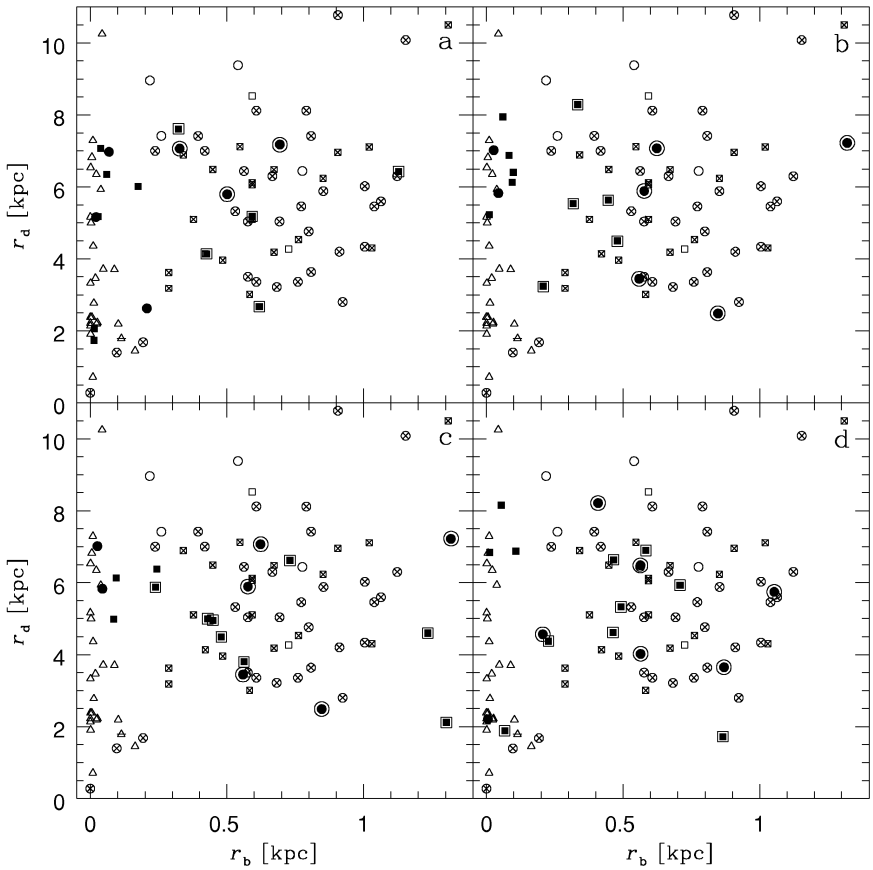


**Figure 10.** Distribution of bulge and disc scalelengths for the simulated galactic objects at $z_A$ (a), $z_B$ (b), $z_C$ (c) and $z_D$ (d). Different symbols have been used to distinguish between $n \leqslant 1.5$ (encircled symbols) and $n > 1.5$, and between double (filled squares) and single (filled circles) starbursts. Observational data from MGH99 ($n = 1$ crossed squares, $n = 2$: open squares), KWK00 ($n \leqslant 1.5$: crossed-triangles, $n > 1.5$: open triangles) and MCH02 ($n \leqslant 1.5$: crossed-circles, $n > 1.5$: open circles) are also shown.

In Fig. 11 we show the $B/D$ ratio for the simulated GLOs during merger events at the four redshifts of interest and the observational data from APB95, KWK00 and MCH02. The low statistical number restricts the use of linear regression through the simulated data. However, we see that, at any time during merger events, the simulated values are within the observational range.

In Fig. 12 we plot the variations $n_{z_i} - n_{z_j}$ versus $B/D_{z_i} - B/D_{z_j}$, where $i/j$ can be A, C or D. From this figure we see that GLOs that experience gas inflows show more important changes in both $n$ and $B/D$ during the ODP. In the case of those GLOs experiencing SSBs (e.g. no early gas inflows) there is no important change in the shape parameter or the $B/D$ ratios during the ODP. We also note that the changes in $n$ and $B/D$ do not correlate. Conversely, during the actual fusion of the objects (from $z_C$ to $z_D$) both types of GLO experience large changes in both parameters in the expected direction: the larger the increase in the shape parameter, the larger the corresponding increase of the $B/D$ ratio or vice versa. Fig. 12(c) shows the overall changes over the merger events. This distribution has a higher dispersion than that obtained during the fusions because it also combines the effects of secular evolution. However, the overall effect of mergers is to settle the correlation between $B/D$ and $n$ so that more concentrated bulges (higher shape parameters) have the larger $B/D$ ratios. However, we note that, although the range of values can be matched, the simulated $B/D$ do not show the same correlation signal ($r = 0.20$) as the observations ($r = 0.55$).

## 4 CONCLUSIONS

We have studied the properties of the baryon distributions in galaxy-like objects focusing on the effects of mergers. We resort to observations of spiral galaxies of different morphology to constrain our findings.

We found that on average, galactic objects formed in hierarchical clustering scenarios reproduce the angular momentum and structural parameter distributions of spiral galaxies, if a stellar bulge is allowed to form and early gas depletion is avoided. We have succeeded in these two aspects but at the expense of inhibiting star formation on discs. A consistent treatment of energy feedback may help to remove this caveat.

These simulations have allowed us to study how mergers change the distribution of baryons by analysing the evolution of their structural parameters. We found that, on average, galactic objects tend to have nearly exponential bulges at all redshift. However, note that these simulations produce bulges with shape parameters in the range 0.5–4.

For those systems with $n \approx 1$ bulges we found a correlation among their bulge and disc scalelengths in very good agreement with observations. However, for $n > 1$ the scalelength distribution is disordered and displaced to smaller bulge scalelengths. Observations show the same behaviour. The opposite distribution is found for systems with $n < 1$ bulges, which have larger $r_b/r_d$ values and larger dispersions. We found the disc scalelengths to be

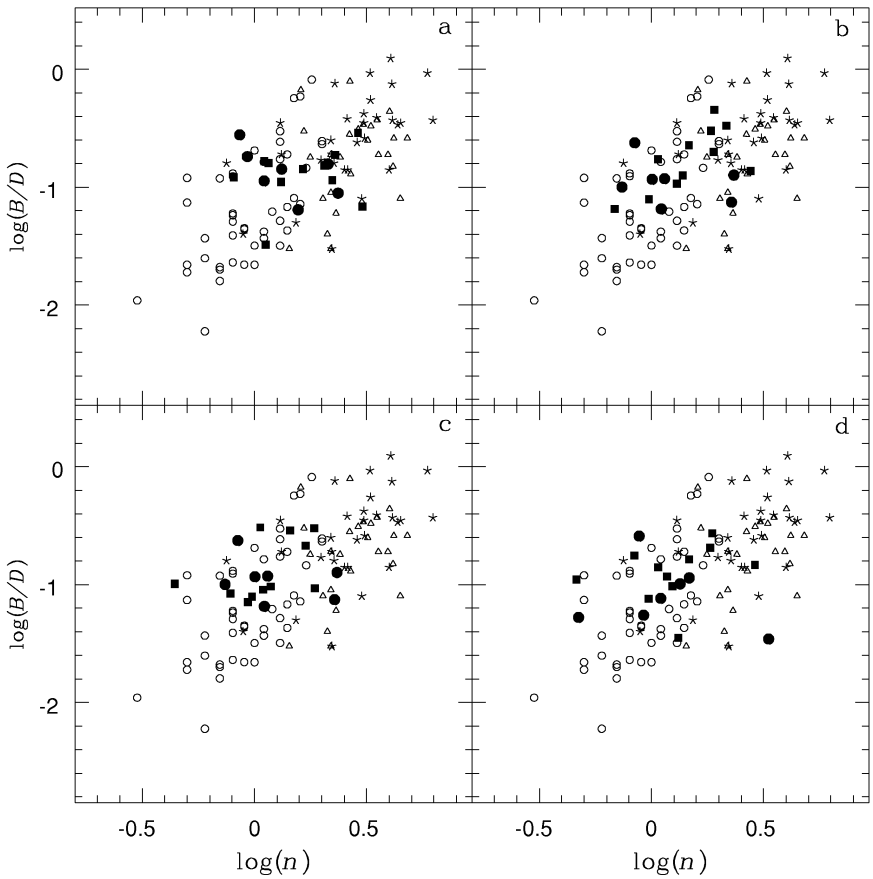


**Figure 11.** Luminosity bulge-to-disc ratio ($B/D$) as a function of the shape parameter of the progenitors during single (filled circles) and double (filled squares) SBs at $z_A$ (a), $z_B$ (b), $z_C$ (c) and $z_D$ (d). Observational data from APB95 (asterisks), KWK00 (open triangles) and MCH02 (open circles) are also shown.

approximately independent of $n$ parameters, so that this correlation implies that more concentrated objects have smaller bulge scalelengths (or large effective radius). We also found a maximum $r_b/r_d$ of $\approx$0.40 for $n \to 0$. Higher numerical resolution simulations are needed to study the formation of such low-mass surface profiles.

In order to test our results for low-resolution problems in the determination of the structural parameters of the galaxy-like objects, we followed Steinmetz & Müller (1994) and used the bootstrap technique to estimate the effects of low particle number statistics within the objects. We calculated an accuracy of better than 25 per cent for the scalelengths and shape parameters.

We found that gas inflows during the orbital decay phase tend to produce important changes in the mass distributions generating $n \approx 1$ profiles, while the fusions of the baryonic cores tend to increase the $n$ parameter. Consequently, a morphological loop can be driven by mergers, which might be responsible for triggering secular evolution and of the baryonic core fusions. The triggering of secular evolution is found to be linked to the presence of a stellar bulge so that systems with well-formed stellar bulges do not experience early gas inflows. Hence, the pace of this morphological loop could be regulated by the properties of the galactic central potential wells, which are also affected by the merger history of the objects (see also Tissera & Domínguez-Tenreiro 1998; Tissera 2000).

We found that the simulated mass bulge-to-disc ratios are within the observed range. It is also noted that during the ODP larger changes are observed in the $B/D$ ratios of those objects that experience gas inflows. The changes during this period are, however, quite disordered. It is at the fusion of the baryonic clumps that changes in the shape parameters are correlated with changes in the bulge-to-disc ratio. In our simulations, the actual fusions are responsible for significantly increasing the mass concentration at the centre. Hence, we found that the fusion of the baryonic cores could be the process that determines the observed correlation between the luminosity $B/D$ ratio and the shape parameter or morphological type. However, we found no dependence on the relative masses of the colliding objects.

Overall, our results indicate that the morphological properties of galactic objects are the result of their merger histories within a hierarchical clustering scenario. Based on the good agreement found so far with observations we support the hypothesis of mergers as the main morphological driver along the Hubble sequence. Consequently, the particular and detailed history of substructure aggregation could be a key point in the determination of the astrophysical properties of galaxies.

## ACKNOWLEDGMENTS

We thank the anonymous referee for useful comments that helped to improve this paper. We are grateful to S. Courteau and his collaborators for making available their observational data prior to publication. We acknowledge A. Graham and S. Courteau for useful discussions. We thank the Max-Planck Institute for Astrophysics

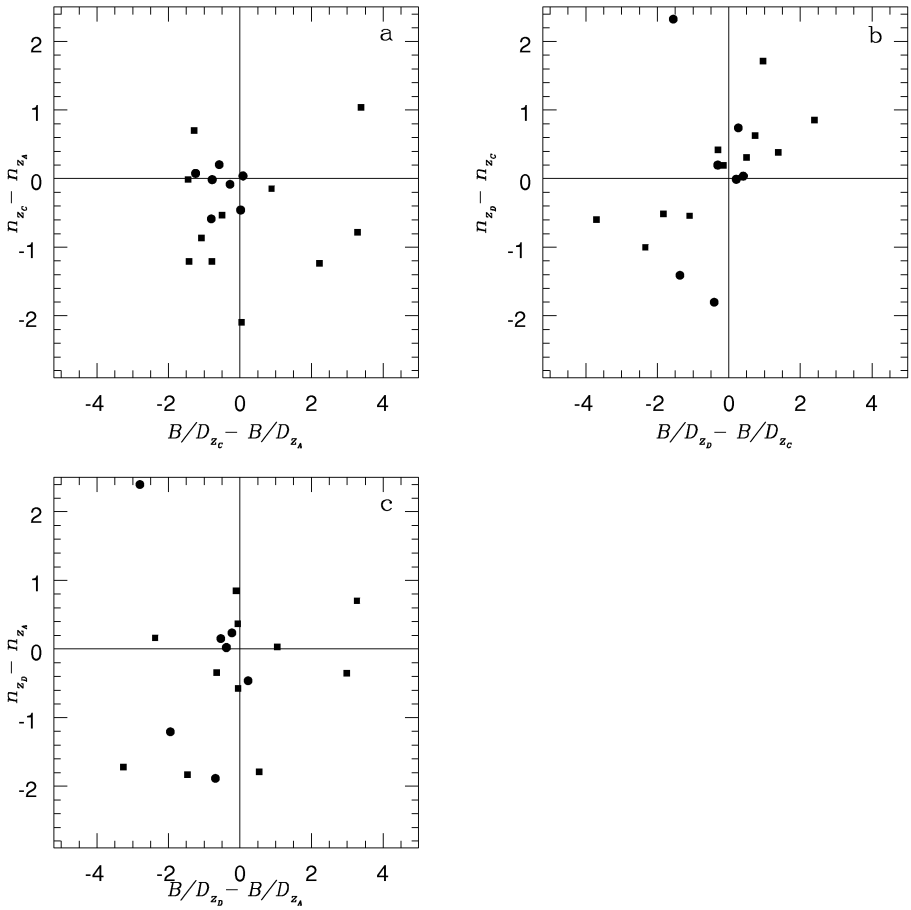


**Figure 12.** Variations in the shape parameters of the progenitors during the orbital decay phase (a), the fusion of the baryonic clumps (b) and the whole merger process (c) in single (filled circles) and double (filled squares) SBs as a function of the corresponding changes in the bulge-to-disc ratio, $B/D$.

for their hospitality, where this paper was completed. This work was partially supported by the Consejo Nacional de Investigaciones Científicas y Técnicas, Agencia de Promoción de Ciencia y Tecnología and Fundación Antorchas.

## REFERENCES

Aguerri J.A.L., Balcells M., Peletier R.F., 2001, A&A, 367, 428 (A01)
Andredakis Y.C., Sanders R.H., 1994, MNRAS, 267, 283
Andredakis Y.C., Peletier R.F., Balcells M., 1995, MNRAS, 275, 874 (APB95)
Barnes J.E., Hernquist L., 1996, ApJ, 471, 115
Ciotti L., Bertin G., 1999, A&A, 353, 447
Courteau S., de Jong R.S., Broeils A.H., 1996, ApJ, 457, L73 (CdJB96)
Dalcanton J.J., Spergel D.N., Summers F.J., 1997, ApJ, 480, L91
de Jong R.S., 1996, A&A, 313, 45
Domínguez-Tenreiro R., Tissera P.B., Sáiz A., 1998, ApJ, 508, L123 (DT98)
Fall S.M., 1983, in Athanssoula E., eds, Proc. IAU Symp. 100, Internal Kinematics and Dynamics of Galaxies. Reidel, Dordrecht, p. 391
Fall S.M., Efstathiou G., 1980, MNRAS, 193, 189 (FE80)
Gilmore G., Wyse R.F.G., 1998, AJ, 116, 748
Graham A.W., de Blok W.J.G., 2001, ApJ, 556, 177 (GdB01)
Graham A.W., Prieto M., 1999, ApJ, 524, L23 (GP99)
Kauffmann G., Guiderdoni B., White S.D.M., 1994, MNRAS, 267, 981
Khosroshahi H.G., Wadadekar Y., Kembhavi A., 2000, ApJ, 533, 162 (KWK00)
MacArthur L.A., Courteau S., Holtzman J.A., 2002, ApJ, (MCH02)
Mihos J.C., Hernquist L., 1994, ApJ, 437, L47
Mihos J.C., Hernquist L., 1996, ApJ, 464, 641
Mo H.J., Mao S., White S.D.M., 1998, MNRAS, 295, 319
Moriondo G., Giovanelli R., Haynes M.P., 1999, A&A, 346, 415 (MGH99)
Navarro J.F., White S.D.M., 1994, MNRAS, 267, 401
Peebles P.J.E., 1969, ApJ, 155, 393
Pfenniger D., Norman C., 1990, ApJ, 363, 391
Sáiz A., Domínguez-Tenreiro R., Tissera P.B., Courteau S., 2001, MNRAS, 325, 119 (S01)
Sérsic J.L., 1968, Atlas de Galaxies Australes. Observatorio Astronómico de Córdoba
Steinmetz M., Müller E., 1994, A&A, 281, L97
Steinmetz M., White S.D.M., 1997, MNRAS, 288, 545
Tissera P.B., 2000, ApJ, 534, 636
Tissera P.B., Domínguez-Tenreiro R., 1998, MNRAS, 297, 177
Tissera P.B., Lambas D.G., Abadi M.G., 1997, MNRAS, 286, 384
Tissera P.B., Domínguez-Tenreiro R., Scannapieco C., Sáiz A., 2002, MNRAS, 333, 327 (T02)
Trujillo I., Graham A.W., Caon N., 2001, MNRAS, 326, 869 (TGC01)
van den Bosch F.C., 1999, in Carollo C.M., Ferguson H.C., Wyse R.F.G., eds, The Formation of Galactic Bulges. Cambridge Univ. Press, Cambridge, p. 50
Weil M.L., Eke V.R., Efstathiou G., 1998, MNRAS, 300, 773

This paper has been typeset from a TEX/LATEX file prepared by the author.